FUNDAMENTALS OF FRACTURE MECHANICS

Dr. Osama Mohammed Elmardi Suleiman Khayal
Department of Mechanical Engineering, Faculty of Engineering and Technology, Nile Valley University, Atbara – Sudan
E – mail address: osamakhayal66@nilevalley.edu.sd

Abstract
Fracture is a problem that society has faced for as long as there have been man-made structures. The problem may actually be worse today than in previous centuries, because more can go wrong in our complex technological society. Major airline crashes, for instance, would not be possible without modern aerospace technology. Fortunately, advances in the field of fracture mechanics have helped to offset some of the potential dangers posed by increasing technological complexity. Our understanding of how materials fail and our ability to prevent such failures have increased considerably since World War II. Much remains to be learned, however, and existing knowledge of fracture mechanics is not always applied when appropriate. While catastrophic failures provide income for attorneys and consulting engineers, such events are detrimental to the economy as a whole. An economic study [1] and [2] estimated the annual cost of fracture in the U.S. in 1978 at $119 billion which was about 4% of the gross national product. Furthermore, this study estimated that the annual cost could be reduced by $35 billion if current technology were applied, and that further fracture mechanics research could reduce this figure by an additional $28 billion. This research paper will introduce several important means of understanding and dealing with fracture in stressed materials.

Keywords: Creep, energy balance, stress intensity, fatigue, fracture

1. Atomistic of Creep Rupture

Creep rupture is a conceptually simple mode of failure in which a specimen is subjected to a constant uniaxial stress at constant temperature and humidity, and the time to fracture recorded. The fact that rupture can occur later and perhaps much later than the time of application of stress implies that fracture is a time dependent process in which damage takes place within the specimen and accumulates until the specimen no longer has sufficient strength to prevent total rupture. As a very simple approach to the damage accumulation process, a first-order mechanism might be proposed in which the number of unbroken bonds decreases at a rate proportional to the number of unbroken bonds remaining:

$$\frac{dn}{dt} = -Kn \longrightarrow \frac{dn}{n} = -K\,dt \longrightarrow n = n_0 e^{-Kt}$$

where n is the fraction of unbroken bonds remaining and K is a rate constant for the process. In such a process the number of unbroken bonds goes to zero only at $t \to \infty$, and clearly fracture will occur well before that. Perhaps a reasonable scaling law would take the creep-rupture lifetime t_f to scale with the average time t for a bond scission, which can be computed as:

$$t_f \approx \langle t \rangle = \frac{\int n \cdot t\,dt}{\int n\,dt} = \frac{1}{K}$$

Following another approach which describes yield as a thermally activated stress aided rate process, the bond scission process is viewed similarly and the rate constant K is written as:

$$K = K_0 \exp \frac{-(E_f^* - \psi V^*)}{kT}$$

where E^* and V^* are an activation energy and volume, and ϕ is the stress on the bond.

Determining ϕ is nontrivial, as ϕ obviously varies over the distribution of bonds and is dependent on the material microstructure. But as another approximation, the atomic stress might be taken to scale with the externally applied stress, giving equation 1 below:

$$\psi \approx \sigma \longrightarrow t_f = t_o \exp \frac{(E_f^* - \sigma V^*)}{kT}$$

where $t_0 = 1/K_0$. A relation similar to this was proposed by S.N. Zhurkov, who conducted a large number of important and innovative studies on the physics of fracture. He argued that fracture is in fact a thermal degradation process, in which an applied stress acts to lower the energy barrier to thermo fluctuation bond dissociation. Fig. 1 shows this relation to describe creep rupture in a wide variety of materials, including ceramics, metals and polymers [3].

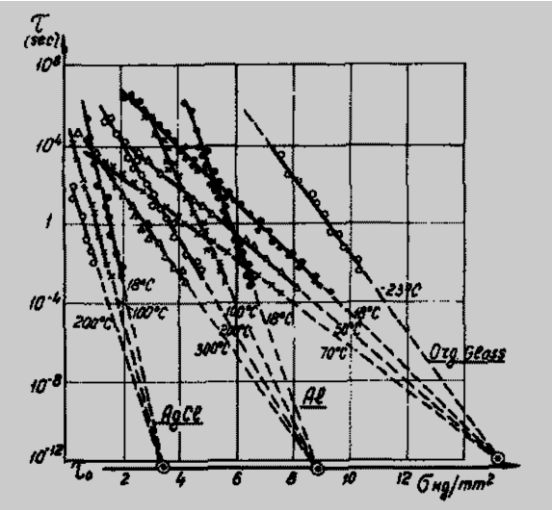

Fig. 1 Time and temperature dependence of the creep-rupture lifetime of solids

2. Fracture Mechanics and the Energy Balance Approach

Failures have occurred for many reasons, including uncertainties in the loading or environment, defects in the materials, inadequacies in design, and deficiencies in construction or maintenance. Design against fracture has a technology of its own, and this is a very active area of current research. This chapter will provide an introduction to an important aspect of this field, since without an understanding of fracture the elaborate methods in stress analysis now available would be of little use. The focus will be on fractures due to simple tensile overstress, but the designer is cautioned about the need to consider absolutely as many factors as possible that might lead to failure, especially when life is at risk.

The strength of structural metals particularly steel can be increased to very high levels by manipulating the microstructure so as to inhibit dislocation motion. Unfortunately, this renders the material increasingly brittle, so that cracks can form and propagate catastrophically with very little warning. An unfortunate number of engineering disasters are related directly to this phenomenon, and engineers involved in structural design must be aware of the procedures now available to safeguard against brittle fracture.

The central difficulty in designing against fracture in high-strength materials is that the presence of cracks can modify the local stresses to such an extent that the elastic stress analyses done so carefully by the designers are insufficient. When a crack reaches a certain critical length, it can propagate catastrophically through the structure, even though the gross stress is much less than would normally cause yield or failure in a tensile specimen. The term fracture mechanics refers to a vital specialization within solid mechanics in which the presence of a crack is assumed, and quantitative relations should be found between the crack length, the material inherent resistance to crack growth, and the stress at which the crack propagates at high speed to cause structural failure.

When A.A. Griffith (1893–1963) began his pioneering studies of fracture in glass in the years just prior to 1920, he was aware of Inglis' work [4] in calculating the stress concentrations around elliptical holes, and naturally considered how it might be used in developing a fundamental approach to predicting fracture strengths. However, the Inglis solution poses a mathematical difficulty: in the limit of a perfectly sharp crack, the stresses approach infinity at the crack tip. This is obviously nonphysical (actually the material generally undergoes some local yielding to blunt the crack tip), and using such a result would predict that materials would have near-zero strength: even

for very small applied loads, the stresses near crack tips would become infinite, and the bonds there would rupture. Rather than focusing on the crack-tip stresses directly, Griffith employed an energy-balance approach that has become one of the most famous developments in materials science [5]. The strain energy per unit volume of stressed material is:

$$U^* = \frac{1}{V}\int f\,dx = \int \frac{f}{A}\frac{dx}{L} = \int \sigma d\epsilon$$

If the material is linear (σ = Eε), then the strain energy per unit volume is:

$$U^* = \frac{E\epsilon^2}{2} = \frac{\sigma^2}{2E}$$

When a crack has grown into a solid to a depth a, a region of material adjacent to the free surfaces is unloaded, and its strain energy released. Using the Inglis solution, Griffith was able to compute just how much energy this is.

A simple way of visualizing this energy release, illustrated in Fig. 2, is to regard two triangular regions near the crack flanks, of width a and height βa, as being completely unloaded, while the remaining material continues to feel the full stress σ. The parameter β can be selected so as to agree with the Inglis solution, and it turns out that for plane stress loading β = π. The total strain energy U released is then the strain energy per unit volume times the volume in both triangular regions:

$$U = -\frac{\sigma^2}{2E}\cdot \pi a^2$$

Here the dimension normal to the x-y plane is taken to be unity, so U is the strain energy released per unit thickness of specimen. This strain energy is liberated by crack growth. But in forming the crack, bonds must be broken, and the requisite bond energy is in effect absorbed by the material. The surface energy S associated with a crack of length a (and unit depth) is:

$$S = 2\gamma a$$

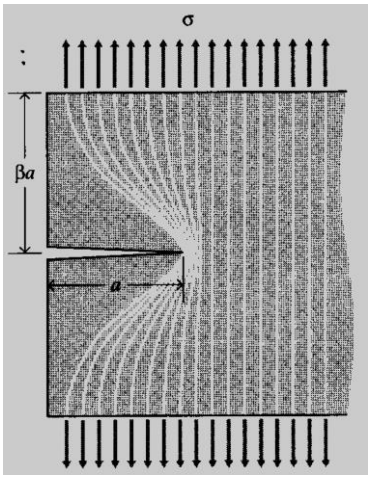

Fig. 2 Idealization of unloaded region near crack flanks

where γ is the surface energy (e.g., Joules/meter^2) and the factor 2 is needed since two free surfaces have been formed. As shown in Fig. 3, the total energy associated with the crack is then the sum of the (positive) energy absorbed to create the new surfaces, plus the (negative) strain energy liberated by allowing the regions near the crack flanks to become unloaded.

As the crack grows longer (a increases), the quadratic dependence of strain energy on a eventually dominates the surface energy, and beyond a critical crack length a_c the system can lower its energy by letting the crack grow still longer. Up to the point where a = a_c, the crack will grow only if the stress in increased. Beyond that point, crack growth is spontaneous and catastrophic.

The value of the critical crack length can be found by setting the derivative of the total energy S + U to zero:

$$\frac{\partial(S+U)}{\partial a} = 2\gamma - \frac{\sigma_f^2}{E}\pi a = 0$$

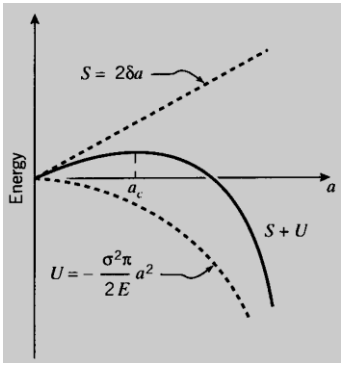

Fig. 3 The fracture energy balance

Since fast fracture is imminent when this condition is satisfied, we write the stress as σ_f . Solving,

$$\sigma_f = \sqrt{\frac{2E\gamma}{\pi a}}$$

Griffith original work dealt with very brittle materials, specifically glass rods. When the material exhibits more ductility, consideration of the surface energy alone fails to provide an accurate model for fracture. This deficiency was later remedied, at least in part, independently by Irwin [6] and Orowan [7]. They suggested that in a ductile material a good deal in fact was the vast majority of the released strain energy which was absorbed not by creating new surfaces, but by energy dissipation due to plastic flow in the material near the crack tip. They suggested that catastrophic fracture occurs when the strain energy is released at a rate sufficient to satisfy the needs of all these energy sinks, and denoted this critical strain energy release rate by the parameter G_c; the Griffith equation can then be rewritten in the following form (equation 2):

$$\sigma_f = \sqrt{\frac{EG_c}{\pi a}}$$

This expression describes, in a very succinct way, the interrelation between three important aspects of the fracture process: the material, as evidenced in the critical strain energy release rate G_c; the stress level σ_f; and the size, a, of the flaw. In a design situation, one might choose a value of a based on the smallest crack that could be easily detected. Then for a given material with its associated value of G_c, the safe level of stress σ_f could be determined. The structure would then be sized so as to keep the working stress comfortably below this critical value.

Example 1:

The story of the De Havilland Comet aircraft of the early 1950^S, in which at least two aircraft disintegrated in flight, provides a tragic but fascinating insight into the importance of fracture theory. It is an eerie story as well, having been all but predicted in a 1948 novel by Nevil Shute named No Highway. The book later became a movie starring James Stewart as a perseverant metallurgist convinced that his company new aircraft (the Reindeer) was fatally prone to metal fatigue. When just a few years later the Comet was determined to have almost exactly this problem, both the book and the movie became rather famous in the materials engineering community.

The postmortem study of the Comet problems was one of the most extensive in engineering history [8]. It required salvaging almost the entire aircraft from scattered wreckage on the ocean floor and also involved full-scale pressurization of an aircraft in a giant water tank. Although valuable lessons were learned, it is hard to overstate the damage done to the De Havilland Company and to the British aircraft industry in general. It is sometimes argued that the long predominance of the United States in commercial aircraft is due at least in part to the Comet misfortune.

The Comet aircraft had a fuselage of clad aluminum, with $G_c \approx 300$ in-psi. The hoop stress due to relative cabin pressurization was 20,000 psi, and at that stress the length of crack that will propagate catastrophically is:

$$a = \frac{\mathcal{G}_c E}{\pi \sigma^2} = \frac{(300)(11 \times 10^6)}{\pi (20 \times 10^3)^2} = 2.62''$$

A crack would presumably be detected in routine inspection long before it could grow to this length. But in the case of the Comet, the cracks were propagating from rivet holes near the cabin windows. When the crack reached the window, the size of the window opening was effectively added to the crack length, leading to disaster.

Modern aircraft are built with this failure mode in mind, and have "tear strips" that are supposedly able to stop any rapidly growing crack. But this remedy is not always effective, as was demonstrated in 1988 when a B737 operated by Aloha Airlines had the roof of the first class cabin tear away. That aircraft had stress-corrosion damage at a number of rivets in the fuselage lap splices, and this permitted multiple small cracks to link up to form a large crack. A great deal of attention is currently being directed to protection against this sort of multi-site damage.

It is important to realize that the critical crack length is an absolute number, not depending on the size of the structure containing it. Each time the crack jumps ahead, say by a small increment δ_a, an additional quantity of strain energy is released from the newly-unloaded material near the crack. Again using our simplistic picture of a triangular-shaped region that is at zero stress while the rest of the structure continues to feel the overall applied stress. It is easy to see in Fig. 4 that much more energy is released due to the jump at position 2 than at position 1. This is yet another reason why small things tend to be stronger: they simply aren't large enough to contain a critical-length crack.

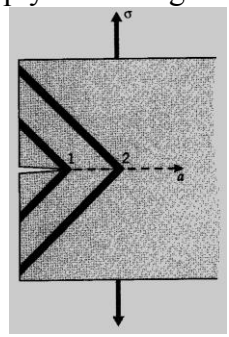

Fig. 4 Energy released during an increment of crack growth, for two different crack lengths

Example 2:

Gordon [9] and [10] tells of a ship cook who one day noticed a crack in the steel deck of his galley. His superiors assured him that it was nothing to worry about because the crack was certainly small compared with the vast bulk of the ship but the cook began painting dates on the floor to mark the new length of the crack each time a bout of rough weather would cause it to grow longer. With each advance of the crack, additional decking material was unloaded, and the strain energy formerly contained in it released. But as the amount of energy released grows quadratically with the crack length, eventually enough was available to keep the crack growing even with no further increase in the gross load. When this happened, the ship broke into two pieces; this seems amazing but there are a more than a few such occurrences that are very well documented. As it happened, the part of the ship with the marks showing the crack's growth was salvaged, and this has become one of the very best documented examples of slow crack growth followed by final catastrophic fracture.

A. Compliance Calibration

A number of means are available by which the material property G_c can be measured. One of these is known as compliance calibration, which employs the concept of compliance as a ratio of deformation to applied load: $C = \delta/P$. The total strain energy U can be written in terms of this compliance as:

$$U = \frac{1}{2} P\delta = \frac{1}{2} CP^2$$

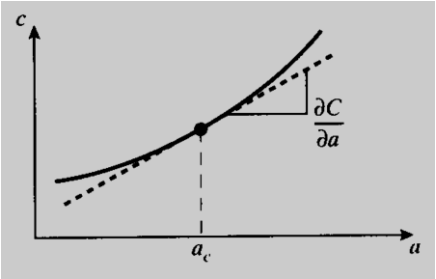

Fig. 5 Compliance as a function of crack length

The compliance of a suitable specimen, for instance a cantilevered beam, could be measured experimentally as a function of the length a of a crack that is grown into the specimen (see Fig. 5). The strain energy release rate can then be determined by differentiating the curve of compliance versus length: (equations 3 and 4 below).

$$\mathcal{G} = \frac{\partial U}{\partial a} = \frac{1}{2}P^2\frac{\partial C}{\partial a}$$

The critical value of G, G_c, is then found by measuring the critical load P_c needed to fracture a specimen containing a crack of length ac, and using the slope of the compliance curve at this same value of a:

$$\mathcal{G}_c = \frac{1}{2}P_c^2\frac{\partial C}{\partial a}\bigg|_{a=a_c}$$

Example 3:

For a double cantilever beam (DCB) specimen such as that shown in Fig. 6, beam theory gives the deflection as:

$$\frac{\delta}{2} = \frac{Pa^3}{3EI}$$

where $I = bh^3/12$. The elastic compliance is then:

$$C = \frac{\delta}{P} = \frac{2a^3}{3EI}$$

If the crack is observed to jump forward when P = Pc, Eqn. 6.4 can be used to compute the critical strain energy release rate as:

$$\mathcal{G}_c = \frac{1}{2}P_c^2 \cdot \frac{2a^2}{EI} = \frac{12P_c^2a^2}{b^2h^3E}$$

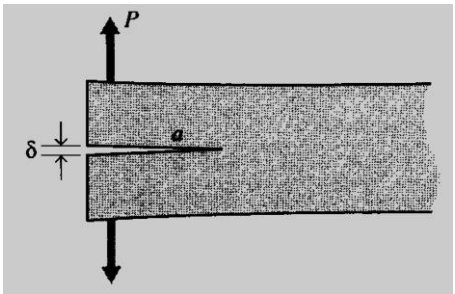

Fig. 6 DCB fracture specimen

3. The Stress Intensity Approach

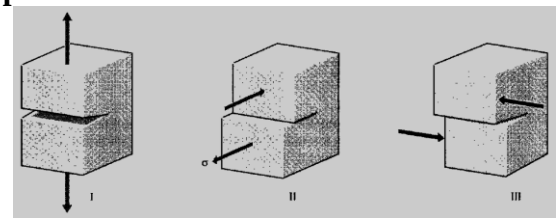

Fig. 7 Fracture modes

While the energy-balance approach provides a great deal of insight to the fracture process, an alternative method that examines the stress state near the tip of a sharp crack directly has proven more useful in engineering practice. The literature treats three types of cracks, termed mode I, II, and III as illustrated in Fig. 7. Mode I is a normal-opening mode and is the one we shall emphasize here, while modes II and III are shear sliding modes. The "semi-inverse" method developed by Westergaard [11] shows the opening-mode stresses to be: (equation 5 below).

$$\sigma_x = \frac{K_I}{\sqrt{2\pi r}} \cos\frac{\theta}{2}\left(1 - \sin\frac{\theta}{2}\sin\frac{3\theta}{2}\right) + \dots$$

$$\sigma_y = \frac{K_I}{\sqrt{2\pi r}} \cos\frac{\theta}{2}\left(1 + \sin\frac{\theta}{2}\sin\frac{3\theta}{2}\right) + \dots$$

$$\tau_{xy} = \frac{K_I}{\sqrt{2\pi r}} \cos\frac{\theta}{2}\cos\frac{3\theta}{2}\sin\frac{\theta}{2} \dots$$

For distances close to the crack tip ($r \leq 0.1a$), the second and higher order terms indicated by dots may be neglected. At large distances from the crack tip, these relations cease to apply and the stresses approach their far-field values that would obtain were the crack not present.

The K_I in Equations 5 is a very important parameter known as the stress intensity factor. The I subscript is used to denote the crack opening mode, but similar relations apply in modes II and III. The equations show three factors that taken together depict the stress state near the crack tip: the denominator factor $(2\pi r)^{-1/2}$ shows the singular nature of the stress distribution; σ approaches infinity as the crack tip is approached, with a $r^{-1/2}$ dependency. The angular dependence is separable as another factor; e.g. $f_x = \cos\theta/2 \times (1 - \sin\theta/2 \sin 3\theta/2)$ + etc. The factor K_I contains the dependence on applied stress σ_∞, the crack length a, and the specimen geometry. The K_I factor gives the overall intensity of the stress distribution, hence its name.

For the specific case of a central crack of width 2a or an edge crack of length 2a in a large sheet, $K_I = \sigma_\infty \sqrt{\pi a}$, and $K_I = 1.12\sigma_\infty \sqrt{\pi a}$ for an edge crack of length a in the edge of a large sheet. (The factor π could obviously be canceled with the π in the denominator of equation 5, but is commonly retained for consistency with earlier work.) Expressions for K_I for some additional geometries are given in Table 6.1. The literature contains expressions for K for a large number of crack and loading geometries, and both numerical and experimental procedures exist for determining the stress intensity factor is specific actual geometries.

Table 1 Stress intensity factors for several common geometries

Type of Crack	Stress Intensity Factor, K_I
Center crack, length $2a$, in an infinite plate	$\sigma_\infty\sqrt{\pi a}$
Edge crack, length a, in a semi-infinite plate	$1.12\ \sigma_\infty\sqrt{\pi a}$
Central penny-shaped crack, radius a, in in infinite body	$2\ \sigma_\infty\sqrt{\frac{a}{\pi}}$
Center crack, length $2a$ in plate of width W	$\sigma_\infty\sqrt{W\tan\left(\frac{\pi a}{W}\right)}$
2 symmetrical edge cracks, each length a, in plate of total width W	$\sigma_\infty\sqrt{W\left[\tan\left(\frac{\pi a}{W}\right) + 0.1\sin\left(\frac{2\pi a}{W}\right)\right]}$

These stress intensity factors are used in design and analysis by arguing that the material can withstand crack tip stresses up to a critical value of stress intensity, termed K_{Ic}, beyond which the crack propagates rapidly. This critical stress intensity factor is then a measure of material toughness.

The failure stress σ_f is then related to the crack length a and the fracture toughness by equation 6 below.

$$\sigma_f = \frac{K_{Ic}}{\alpha\sqrt{\pi a}}$$

where α is a geometrical parameter equal to 1 for edge cracks and generally on the order of unity for other situations. Expressions for α are tabulated for a wide variety of specimen and crack geometries, and specialty finite element methods are available to compute it for new situations. The stress intensity and energy viewpoints are interrelated, as can be seen by comparing equations 2 and 6 (with α = 1):

$$\sigma_f = \sqrt{\frac{E\mathcal{G}_c}{\pi a}} = \frac{K_{Ic}}{\sqrt{\pi a}} \rightarrow K_{Ic}^2 = E\mathcal{G}_c$$

This relation applies in plane stress; it is slightly different in plane strain:

$$K_{Ic}^2 = E\mathcal{G}_c(1-\nu^2)$$

For metals with ν = .3, $(1-\nu^2)$ = 0.91. This is not a big change; however, the numerical values of G_c or K_{Ic} are very different in plane stress or plane strain situations, as will be described below. Typical values of G_{Ic} and K_{Ic} for various materials are listed in Table 2, and it is seen that they vary over a very wide range from material to material. Some polymers can be very tough, especially when rated on a per-pound bases, but steel alloys are hard to beat in terms of absolute resistance to crack propagation.

Table 2 Fracture toughness of materials

Material	G_{Ic}(kJm^{-2})	K_{Ic}(MPam$^{1/2}$)	E(GPa)
Steel alloy	107	150	210
Aluminum alloy	20	37	69
Polyethylene	20 (J_{Ic})	—	0.15
High-impact polystyrene	15.8 (J_{Ic})	—	2.1
Steel — mild	12	50	210
Rubber	13	—	0.001
Glass-reinforced thermoset	7	7	7
Rubber-toughened epoxy	2	2.2	2.4
PMMA	0.5	1.1	2.5
Polystyrene	0.4	1.1	3
Wood	0.12	0.5	2.1
Glass	0.007	0.7	70

Example 4

Equation 6 provides a design relation among the applied stress σ, the material's toughness K_{Ic}, and the crack length a. Any one of these parameters can be calculated once the other two are known. To illustrate one application of the process, say we wish to determine the safe operating pressure in an aluminum pressure vessel 0.25 m in diameter and with a 5 mm wall thickness. First assuming failure by yield when the hoop stress reaches the yield stress (330 MPa) and using a safety factor of 0.75, we can compute the maximum pressure as:

$$p = \frac{0.75\sigma t}{r} = \frac{0.75 \times 330 \times 10^6}{0.25/2} = 9.9 \text{ MPa} = 1400 \text{ psi}$$

To insure against failure by rapid crack growth, we now calculate the maximum crack length permissible at the operating stress, using a toughness value of KIc = 41 MPa $\sqrt{}$m:

$$a = \frac{K_{Ic}^2}{\pi\sigma^2} = \frac{(41 \times 10^6)^2}{\pi\,(0.75 \times 330 \times 10^6)^2} = 0.01 \text{ m} = 0.4 \text{ in}$$

Here an edge crack with α = 1 has been assumed. An inspection schedule must be implemented that is capable of detecting cracks before they reach this size.

A. Effect of Specimen Geometry

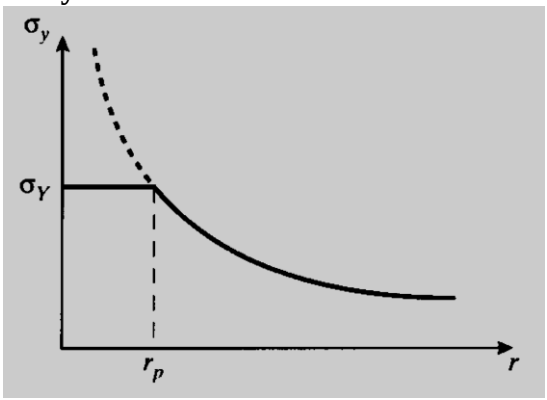

Fig. 8 Stress limited by yield within zone r_p

The toughness, or resistance to crack growth, of a material is governed by the energy absorbed as the crack moves forward. In an extremely brittle material such as window glass, this energy is primarily just that of rupturing the chemical bonds along the crack plane. But as already mentioned, in tougher materials bond rupture plays a relatively small role in resisting crack growth, with by far the largest part of the fracture energy being associated with plastic flow near the crack tip. A plastic zone is present near the crack tip within which the stresses as predicted by equation 5 would be above the material's yield stress σ_Y . Since the stress cannot rise above σ_Y , the stress in this zone is σ_Y rather than that given by equation 5. To a first approximation, the distance r_p this zone extends along the x-axis can be found by using equation 5 with $\theta = 0$ to find the distance at which the crack tip stress reduces to σ_Y : equation 7 below.

$$\sigma_y = \sigma_Y = \frac{K_I}{\sqrt{2\pi r_p}}$$

$$r_p = \frac{K_I^2}{2\pi\sigma_Y^2}$$

This relation is illustrated in Fig. 8. As the stress intensity in increased either by raising the imposed stress or by crack lengthening, the plastic zone size will increase as well. But the extent of plastic flow is ultimately limited by the material's molecular or microstructural mobility, and the zone can become only so large. When the zone can grow no larger, the crack can no longer be constrained and unstable propagation ensues. The value of K_I at which this occurs can then be considered a materials property, named K_{Ic}.

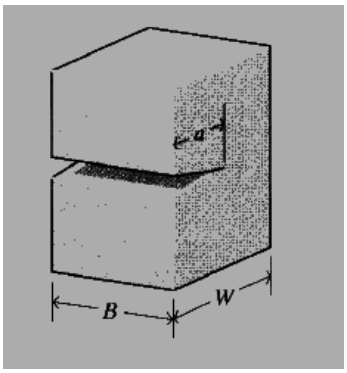

Fig. 9 Dimensions of fracture toughness specimen

In order for the measured value of K_{Ic} to be valid, the plastic zone size should not be so large as to interact with the specimen free boundaries or to destroy the basic nature of the singular stress distribution. The ASTM specification for fracture toughness testing [12] specifies the specimen geometry to insure that the specimen is large compared to the crack length and the plastic zone size (see Fig. 9):

$$a, B, (W-a) \geq 2.5\left(\frac{K_I}{\sigma_Y}\right)^2$$

A great deal of attention has been paid to the important case in which enough ductility exists to make it impossible to satisfy the above criteria. In these cases the stress intensity view must be abandoned and alternative techniques such as the J-integral or the crack tip opening displacement method used instead. The reader is referred to the references listed at the end of the chapter for discussion of these approaches.

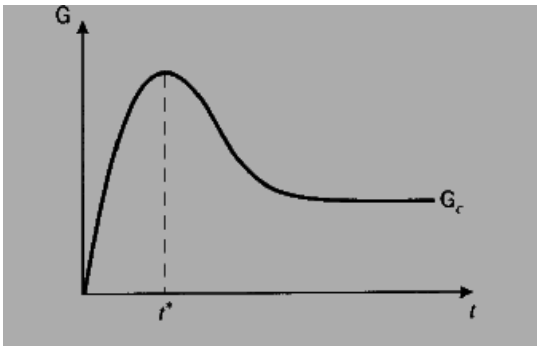

Fig. 10 Effect of specimen thickness on toughness

The fracture toughness as measured by K_c or G_c is essentially a measure of the extent of plastic deformation associated with crack extension. The quantity of plastic flow would be expected to scale linearly with the specimen thickness, since reducing the thickness by half would naturally cut the volume of plastically deformed material approximately in half as well. The toughness therefore rises linearly, at least initially, with the specimen thickness as seen in Fig. 10. Eventually, however, the toughness is observed to go through a maximum and fall thereafter to a lower value. This loss of toughness beyond a certain critical thickness $t*$ is extremely important in design against fracture, since using too thin a specimen in measuring toughness will yield an unrealistically optimistic value for GC. The specimen size requirements for valid fracture toughness testing are such that the most conservative value is measured.

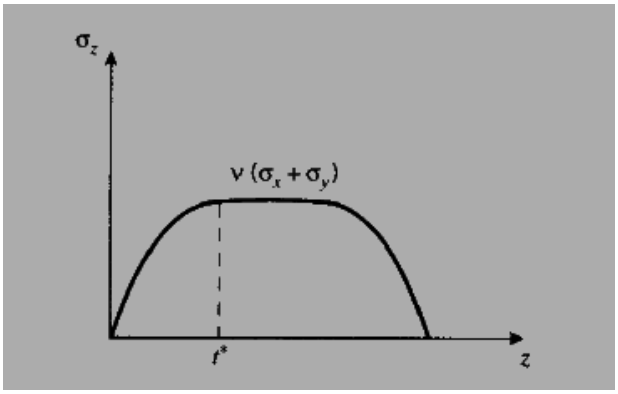

Fig. 11 Transverse stress at crack tip

The critical thickness is that which causes the specimen to be dominated by a state of plane strain, as opposed to plane stress. The stress in the through-thickness z direction must become zero at the sides of the specimen since no traction is applied there, and in a thin specimen the stress will not have room to rise to appreciable values within the material. The strain in the z direction is not zero, of course, and the specimen will experience a Poisson contraction given by $\varepsilon_z = \nu(\sigma_x + \sigma_y)$. But when the specimen is thicker, material near the center will be unable to contract laterally due to the constraint of adjacent material. Now the z-direction strain is zero, so a tensile stress will arise as the material tries to contract but is prevented from doing so. The value of σ_z rises from zero at the outer surface and approaches a maximum value given by $\sigma_z \approx \nu(\sigma_x + \sigma_y)$ in a distance t^* as seen in Fig. 11. To guarantee that plane strain conditions dominate, the specimen thickness t must be such that $t \gg 2t^*$.

The triaxial stress state set up near the center of a thick specimen near the crack tip reduces the maximum shear stress available to drive plastic flow, since the maximum shear stress is equal to one half the difference of the largest and smallest principal stress, and the smallest is now greater than zero. Or equivalently, we can state that the mobility of the material is constrained by the

inability to contract laterally. From either a stress or a strain viewpoint, the extent of available plasticity is reduced by making the specimen thick.

Example 5:

The plastic zone sizes for the plane stress and plane strain cases can be visualized by using a suitable yield criterion along with the expressions for stress near the crack tip. The V. Mises yield criterion was given in terms of principal stresses as in the following equation.

$$2\sigma_Y^2 = (\sigma_1 - \sigma_2)^2 + (\sigma_1 - \sigma_3)^2 (\sigma_2 - \sigma_3)^2$$

The principal stresses can be obtained from equations 5 as follows:

$$\sigma_1 = \frac{K_I}{\sqrt{2\pi r}} \cos\frac{\theta}{2}\left(1 + \sin\frac{\theta}{2}\right)$$

$$\sigma_2 = \frac{K_I}{\sqrt{2\pi r}} \cos\frac{\theta}{2}\left(1 - \sin\frac{\theta}{2}\right)$$

The third principal stress is:

$$\sigma_3 = \begin{cases} 0, & \text{plane stress} \\ \nu(\sigma_1 + \sigma_2), & \text{plane strain} \end{cases}$$

These stresses can be substituted into the yield criterion, which is then solved for the radius r at which yield occurs. It is convenient to normalize this radius by the radius of the plastic zone along the x- axis, given by equation 7.

Even in a thick specimen, the z-direction stress must approach zero at the side surfaces. Regions near the surface are therefore free of the triaxial stress constraint, and exhibit greater shear-driven plastic flow. After a cracked specimen has been tested to failure, a flat “thumbnail” pattern will often be visible as illustrated in Fig. 12. This is the region of slow crack growth, where the crack is able to maintain its preferred orientation transverse to the y-direction stress. The crack growth near the edges is retarded by the additional plastic flow there, so the crack line bows inward. When the stress is increased enough to cause the crack to grow catastrophically, it typically does so at speeds high enough that the transverse orientation is not always maintained. The region of rapid fracture is thus faceted and rough, leading some backyard mechanics to claim the material failed because it crystallized.

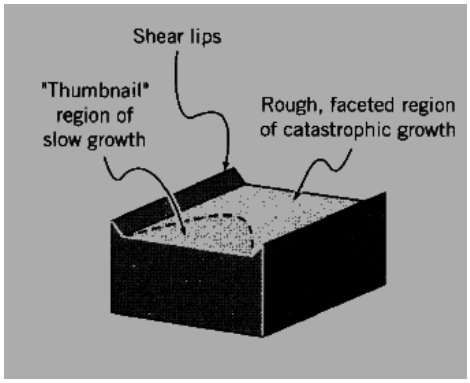

Fig. 12 Fracture surface topography

B. Grain Size and Temperature

Steel is such an important and widely used structural material that it is easy to forget that steel is a fairly recent technological innovation. Well into the nineteenth century, wood was the dominant material for many bridges, buildings, and ships. As the use of iron and steel became more widespread in the latter part of that century and the first part of the present one, a number of disasters took place that can be traced to the then-incomplete state of understanding of these materials, especially concerning their tendency to become brittle at low temperatures. Many of these failures have been described and analyzed in a fascinating book by Parker [13].

One of these brittle failures is perhaps the most famous disaster of the last several centuries, the sinking of the transatlantic ocean liner Titanic on April 15, 1912, with a loss of some 1,500 people and only 705 survivors. Until very recently, the tragedy was thought to be caused by a long gash torn through the ship’s hull by an iceberg. However, when the wreckage of the ship was finally discovered in 1985 using undersea robots, no evidence of such a gash was found. Further, the robots

were later able to return samples of the ship steel whose analysis has given rise to an alternative explanation.

It is now well known that lesser grades of steel, especially those having large concentrations of impurities such as interstitial carbon inclusions, are subject to embrittlement at low temperatures. William Garzke, a naval architect with the New York firm of Gibbs & Cox, and his colleagues have argued that the steel in the Titanic was indeed brittle in the 31°F waters of the Atlantic that night, and that the 22 knot collision with the iceberg generated not a gash but extensive cracking through which water could enter the hull. Had the steel remained tough at this temperature, these authors feel, the cracking may have been much less extensive. This would have slowed the flooding and allowed more time for rescue vessels to reach the scene, which could have increased greatly the number of survivors.

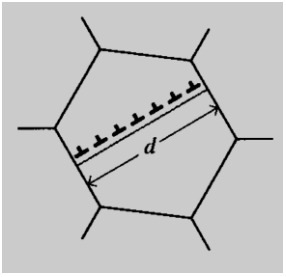

Fig. 13 Dislocation pileup within a grain

In the bcc transition metals such as iron and carbon steel, brittle failure can be initiated by dislocation glide within a crystalline grain. The slip takes place at the yield stress σ_Y , which varies with grain size according to the Hall-Petch law.

$$\sigma_Y = \sigma_0 + k_Y d^{-1/2}$$

Dislocations are not able to propagate beyond the boundaries of the grain, since adjoining grains will not in general have their slip planes suitably oriented. The dislocations then "pile up" against the grain boundaries as illustrated in Fig. 13. The dislocation pileup acts similarly to an internal crack with a length that scales with the grain size d, intensifying the stress in the surrounding grains. Replacing a by d in the modified Griffith equation (equation 2), the applied stress needed to cause fracture in adjacent grains is related to the grain size as:

$$\sigma_f = k_f d^{-1/2}, \quad k_f \propto \sqrt{\frac{E\mathcal{G}_c}{\pi}}$$

The above two relations for yielding and fracture are plotted in Fig. 14 against inverse root grain size (so grain size increases to the left), with the slopes being k_Y and k_f respectively. When $k_f > k_Y$, fracture will not occur until $\sigma = \sigma_Y$ for values of d to the left of point A, since yielding and slip is a prerequisite for cleavage. In this region the yielding and fracture stresses are the same, and the failure appears brittle since large-scale yielding will not have a chance to occur. To the right of point A, yielding takes place prior to fracture and the material appears ductile. The point A therefore defines a critical grain size d^* at which a nil-ductility transition from ductile (grains smaller than d^*) to brittle failure will take place.

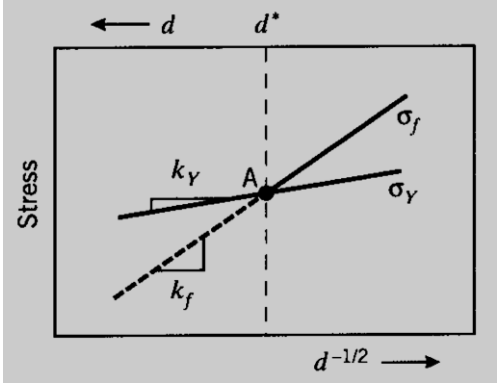

Fig. 14 Effect of grain size on yield and fracture stress

As the temperature is lowered, the yield stress σ_Y will increase as described in Chap. 5, and the fracture stress σ_f will decrease (since atomic mobility and thus G_C decrease). Therefore, point A shifts to the right as temperature is lowered. The critical grain size for nil ductility now occurs at a smaller value; i.e. the grains must be smaller to avoid embrittling the material. Equivalently, refining the grain size has the effect of lowering the ductile-brittle transition temperature. Hence grain-size refinement raises both the yield and fracture stress, lowers the ductile-brittle transition temperature, and promotes toughness as well. This is a singularly useful strengthening mechanism, since other techniques such as strain hardening and solid-solution hardening tend to achieve strengthening at the expense of toughness.

Factors other than temperature can also embrittle steel. Inclusions such as carbon and phosphorus act to immobilize slip systems that might otherwise relieve the stresses associated with dislocation pileups, and these inclusions can raise the yield stress and thus the ductile-brittle transition temperature markedly. Similar effects can be induced by damage from high-energy radiation, so embrittlement of nuclear reactor components is of great concern. Embrittlement is also facilitated by the presence of notches, since they generate triaxial stresses that constrain plastic flow. High strain rates promote brittleness because the flow stress needed to accommodate the strain rate is higher, and improper welding can lead to brittleness both by altering the steel's microstructure and by generating residual internal stresses.

4. Fatigue

The concept of fatigue arose several times in this chapter, as in the growth of cracks in the Comet aircraft that led to disaster when they became large enough to propagate catastrophically as predicted by the Griffith criterion. Fatigue, as understood by materials technologists, is a process in which damage accumulates due to the repetitive application of loads that may be well below the yield point. The process is dangerous because a single application of the load would not produce any ill effects, and a conventional stress analysis might lead to a assumption of safety that does not exist.

In one popular view of fatigue in metals, the fatigue process is thought to begin at an internal or surface flaw where the stresses are concentrated, and consists initially of shear flow along slip planes. Over a number of cycles, this slip generates intrusions and extrusions that begin to resemble a crack. A true crack running inward from an intrusion region may propagate initially along one of the original slip planes, but eventually turns to propagate transversely to the principal normal stress as seen in Fig. 15.

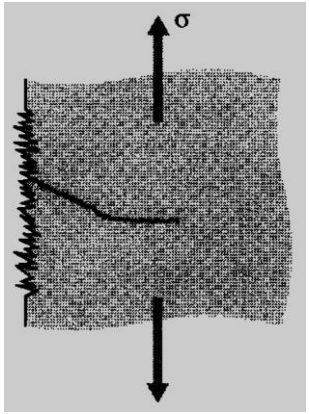

Fig. 15 Intrusion-extrusion model of fatigue crack initiation

When the failure surface of a fatigued specimen is examined, a region of slow crack growth is usually evident in the form of a "clamshell" concentric around the location of the initial flaw. (See Fig. 16). The clamshell region often contains concentric "beach marks" at which the crack was arrested for some number of cycles before resuming its growth. Eventually, the crack may become large enough to satisfy the energy or stress intensity criteria for rapid propagation, following the previous expressions for fracture mechanics. This final phase produces the rough surface typical of fast fracture. In postmortem examination of failed parts, it is often possible to correlate the beach

marks with specific instances of overstress, and to estimate the applied stress at failure from the size of the crack just before rapid propagation and the fracture toughness of the material.

Fig. 16 Typical fatigue-failure surfaces. From B. Chalmers, Physical Metallurgy, Wiley, p. 212, 1959

The modern study of fatigue is generally dated from the work of A. Wohler, a technologist in the German railroad system in the mid-nineteenth century. Wohler was concerned by the failure of axles after various times in service, at loads considerably less than expected. A railcar axle is essentially a round beam in four-point bending, which produces a compressive stress along the top surface and a tensile stress along the bottom (see Fig. 17). After the axle has rotated a half turn, the bottom becomes the top and vice versa, so the stresses on a particular region of material at the surface varies sinusoidally from tension to compression and back again. This is now known as fully reversed fatigue loading.

A. S-N Curves

Well before a microstructural understanding of fatigue processes was developed, engineers had developed empirical means of quantifying the fatigue process and designing against it. Perhaps the most important concept is the S-N diagram, such as those shown in Fig. 18 [14], in which a constant cyclic stress amplitude S is applied to a specimen and the number of loading cycles N until the specimen fails is determined. Millions of cycles might be required to cause failure at lower loading levels, so the abscissa in usually plotted logarithmically.

In some materials, notably ferrous alloys, the S − N curve flattens out eventually, so that below a certain endurance limit σ_e failure does not occur no matter how long the loads are cycled. Obviously, the designer will size the structure to keep the stresses below σ_e by a suitable safety factor if cyclic loads are to be withstood. For some other materials such as aluminum, no endurance limit exists and the designer must arrange for the planned lifetime of the structure to be less than the failure point on the S − N curve.

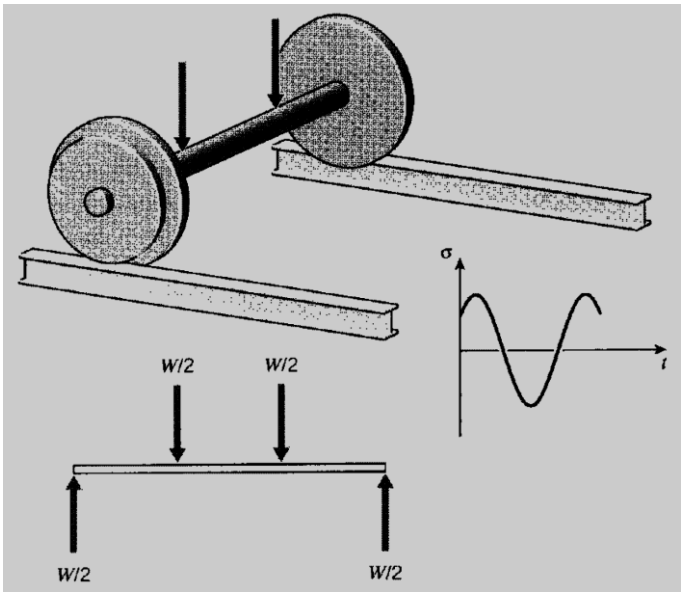

Fig. 17 Fatigue in a railcar axle

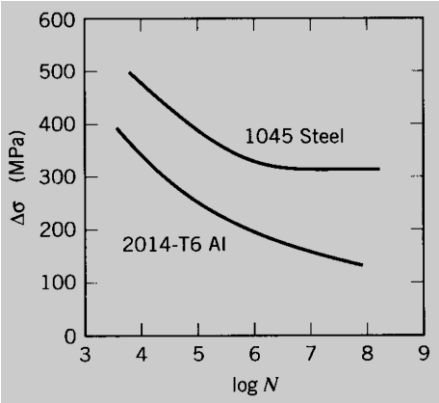

Fig. 18 S − N curves for aluminum and low-carbon steel

Statistical variability is troublesome in fatigue testing; it is necessary to measure the lifetimes of perhaps twenty specimens at each of ten or so load levels to define the S −N curve with statistical confidence [15]. It is generally impossible to cycle the specimen at more than approximately 10Hz (inertia in components of the testing machine and heating of the specimen often become problematic at higher speeds) and at that speed it takes 11.6 days to reach 107 cycles of loading. Obtaining a full S − N curve is obviously a tedious and expensive procedure.

At first glance, the scatter in measured lifetimes seems enormous, especially given the logarithmic scale of the abscissa. If the coefficient of variability in conventional tensile testing is usually only a few percent, then why do the fatigue lifetimes vary over orders of magnitude. It must be remembered that in tensile testing, we are measuring the variability in stress at a given number of cycles (one), while in fatigue we are measuring the variability in cycles at a given stress. Stated differently, in tensile testing we are generating vertical scatter bars, but in fatigue they are horizontal (see Fig. 19). Note that we must expect more variability in the lifetimes as the S − N curve becomes flatter, so that materials that are less prone to fatigue damage require more specimens to provide a given confidence limit on lifetime.

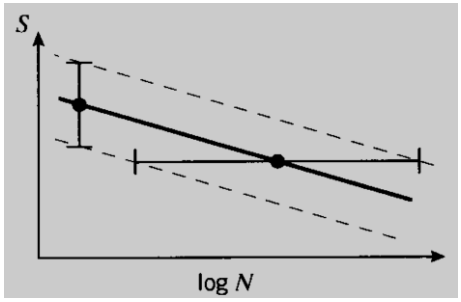

Fig. 19 Variability in fatigue lifetimes and fracture strengths

B. Effect of Mean Load

Of course, not all actual loading applications involve fully reversed stress cycling. A more general sort of fatigue testing adds a mean stress σ_m on which a sinusoidal cycle is superimposed, as shown in Fig. 20. Such a cycle can be phrased in several ways, a common one being to state the alternating stress σ_{alt} and the stress ratio $R = \sigma_{min}/\sigma_{max}$. For fully reversed loading, $R = -1$. A stress cycle of $R = 0.1$ is often used in aircraft component testing, and corresponds to a tension-tension cycle in which $\sigma_{min} = 0.1\sigma_{max}$.

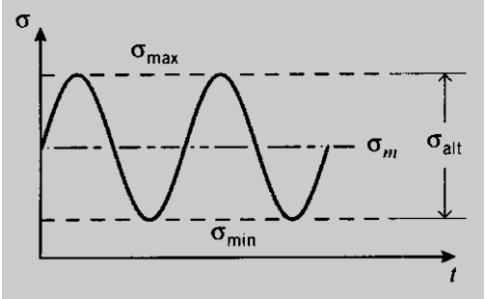

Fig. 20 Simultaneous mean and cyclic loading

A very substantial amount of testing is required to obtain an S −N curve for the simple case of fully reversed loading, and it will usually be impractical to determine whole families of curves for every combination of mean and alternating stress. There are a number of stratagems for finessing this difficulty, one common one being the Goodman diagram. shown in Fig. 21. Here a graph is constructed with mean stress as the abscissa and alternating stress as the ordinate, and a straight "lifeline" is drawn from σ_e on the σ_{alt} axis to the ultimate tensile stress σ_f on the σ_m axis. Then for any given mean stress, the endurance limit is the value of alternating stress at which fatigue fracture never occurs can be read directly as the ordinate of the lifeline at that value of σ_m. Alternatively, if the design application dictates a given ratio of σ_m to σ_{alt}, a line is drawn from the origin with a slope equal to that ratio. Its intersection with the lifeline then gives the effective endurance limit for that combination of σ_f and σ_m.

C. Miner's Law for Cumulative Damage

When the cyclic load level varies during the fatigue process, a cumulative damage model is often hypothesized. To illustrate, take the lifetime to be N_1 cycles at a stress level σ_1 and N_2 at σ_2. If damage is assumed to accumulate at a constant rate during fatigue and a number of cycles n_1 is applied at stress $\sigma 1$, where $n_1 < N_1$ as shown in Fig. 22, then the fraction of lifetime consumed will be n_1/N_1. To determine how many additional cycles the specimen will survive at stress σ_2, an additional fraction of life will be available such that the sum of the two fractions equals one:

$$\frac{n_1}{N_1} + \frac{n_2}{N_2} = 1$$

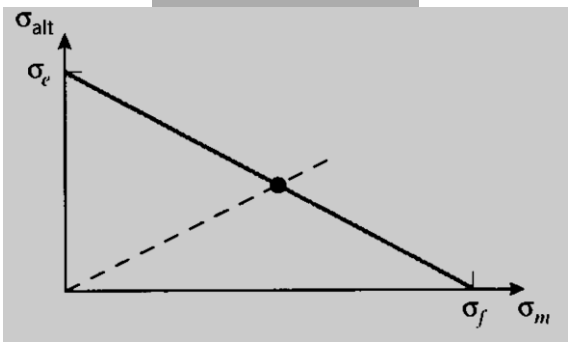

Fig. 21 The Goodman diagram

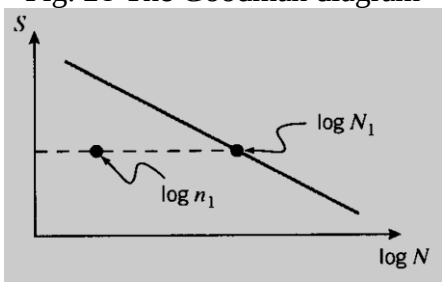

Fig. 22 The concept of fractional lifetime

Note that absolute cycles and not log cycles are used here. Solving for the remaining cycles permissible at σ_2:

$$n_2 = N_2\left(1 - \frac{n_1}{N_1}\right)$$

The generalization of this approach is called Miner's Law, and can be written in equation 8 as follows:

$$\boxed{\sum \frac{n_j}{N_j} = 1}$$

where n_j is the number of cycles applied at a load corresponding to a lifetime of N_j.

Example 6:

Consider a hypothetical material in which the S-N curve is linear from a value equal to the fracture stress σ_f at one cycle (log N = 0), falling to a value of σ_f /2 at log N = 7 as shown in Fig. 23. This behavior can be described by the relation:

$$\log N = 14\left(1 - \frac{S}{\sigma_f}\right)$$

The material has been subjected to $n_1 = 10^5$ load cycles at a level $S = 0.6\sigma_f$, and we wish to estimate how many cycles n_2 the material can now withstand if we raise the load to $S = 0.7\sigma_f$. From the S-N relationship, we know the lifetime at $S = 0.6\sigma f$ = constant would be N1 = 3.98 × 105 and the lifetime at $S = 0.7\sigma_f$ = constant would be $N_2 = 1.58 \times 104$. Now applying equation 8:

$$\frac{n_1}{N_1} + \frac{n_2}{N_2} = \frac{1 \times 10^5}{3.98 \times 10^5} + \frac{n_2}{1.58 \times 10^4} = 1$$

$$n_2 = 1.18 \times 10^4$$

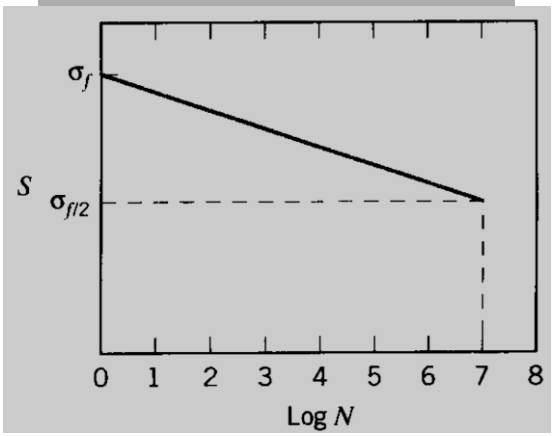

Fig. 23 Linear S-N curve

Miner's law should be viewed like many other material laws, a useful approximation, quite easy to apply, that might be accurate enough to use in design. But damage accumulation in fatigue is usually a complicated mixture of several different mechanisms, and the assumption of linear damage accumulation inherent in Miner's law should be viewed skeptically. If portions of the material's microstructure become unable to bear load as fatigue progresses, the stress must be carried by the surviving microstructural elements. The rate of damage accumulation in these elements then increases, so that the material suffers damage much more rapidly in the last portions of its fatigue lifetime. If on the other hand cyclic loads induce strengthening mechanisms such as molecular orientation or crack blunting, the rate of damage accumulation could drop during some part of the material's lifetime. Miner's law ignores such effects, and often fails to capture the essential physics of the fatigue process.

D. Crack Growth Rates

Certainly in aircraft, but also in other structures as well, it is vital that engineers be able to predict the rate of crack growth during load cycling, so that the part in question be replaced or repaired before the crack reaches a critical length. A great deal of experimental evidence supports the view that the crack growth rate can be correlated with the cyclic variation in the stress intensity factor as shown in equation 9 below:

$$\boxed{\frac{da}{dN} = A\Delta K^m}$$

where da/dN is the fatigue crack growth rate per cycle, $\Delta K = K_{max} - K_{min}$ is the stress intensity factor range during the cycle, and A and m are parameters that depend the material, environment, frequency, temperature and stress ratio. This is sometimes known as the "Paris law," and leads to plots similar to that shown in Fig. 24.

The exponent m is often near 4 for metallic systems, which might be rationalized as the damage accumulation being related to the volume Vp of the plastic zone: since the volume Vp of the zone scales with r^2_p and $r_p \propto K^2_I$, then $da/dn \propto \Delta K^4$. Some specific values of the constants m and A for various alloys in given in Table 3.

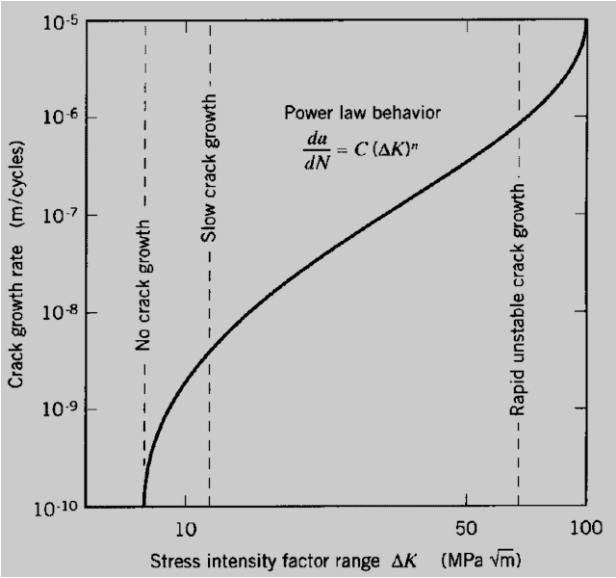

Fig. 24 The Paris law for fatigue crack growth rates

Table 3 Numerical parameters in the Paris equation

alloy	m	A
Steel	3	10^{-11}
Aluminum	3	10^{-12}
Nickel	3.3	4×10^{-12}
Titanium	5	10^{-11}

5. Conclusions

The field of fracture mechanics was virtually nonexistent prior to World War II, but has since matured into an established discipline. Most universities with an engineering program offer at least one fracture mechanics course on the graduate level, and an increasing number of undergraduates have been exposed to this subject. Applications of fracture mechanics in industry are relatively common, as knowledge that was once confined to a few specialists is becoming more widespread. While there are a number of books on fracture mechanics, most are geared to a specific audience.

Some treatments of this subject emphasize material testing, while others concentrate on detailed mathematical derivations. A few books address the microscopic aspects of fracture, but most consider only continuum models. Many books are restricted to a particular material system, such as metals or polymers. Current offerings include advanced, highly specialized books, as well as introductory texts. While the former are valuable to researchers in this field, they are unsuitable for students with no prior background. On the other hand, introductory treatments of the subject are sometimes simplistic and misleading. This research paper provides a comprehensive treatment of fracture mechanics that should appeal to a relatively wide audience. Theoretical background and practical applications are both covered in brief. This research paper is suitable as a graduate text, as well as a reference for engineers and researchers. Selected portions of this research paper would also be appropriate for an undergraduate course in fracture mechanics [16] – [19].

References

[1] Duga, J.J., Fisher, W.H., Buxbaum, R.W., Rosenfield, A.R., Burh, A.R., Honton, E.J., and McMillan, S.C., The Economic Effects of Fracture in the United States. NBS Special Publication 647-2, U.S. Department of Commerce, Washington, DC, March 1983.

[2] R.P. Reed et al., NBS Special Publication 647-1, Washington, 1983.

[3 S.N. Zhurkov, "Kinetic Concept of the Strength of Solids," Int. J. of Fracture Mechanics, Vol. 1, No. 4, pp. 311‑323, Dec. 1965

[4] C.E. Inglis, "Stresses in a Plate Due to the Presence of Cracks and Sharp Corners," Transactions of the Institution of Naval Architects, Vol. 55, London, 1913, pp. 219–230.

[5] A.A. Griffith, Philosophical Transactions, Series A, Vol. 221, pp. 163–198, 1920. The importance of Griffith's work in fracture was largely unrecognized until the 1950's. See J.E. Gordon, The Science of Structures and Materials, Scientific American Library, 1988, for a personal account of the Griffith story.
[6] G.R. Irwin, "Fracture Dynamics," Fracturing of Metals, American Society for Metals, Cleveland, 1948.
[7] E. Orowan, "Fracture and Strength of Solids," Report of Progress in Physics, Vol. 12, 1949.
[8] T. Bishop, Metal Progress, Vol. 67, pp. 79–85, May 1955.
[9] Gordon J.E. , Structures, or Why Things Don't Fall Down, Plenum, New York, 1978.
[10] Gordon, J.E., The New Science of Strong Materials, or Why You Don't Fall Through the Floor, Princeton University Press, 1976.
[11] Westergaard, H.M., "Bearing Pressures and Cracks," Transactions, Am. Soc. Mech. Engrs., Journal of Applied Mechanics, Vol. 5, p. 49, 1939.
[12] E 399-83, "Standard Test Method for Plane-Strain Fracture Toughness of Metallic Materials," ASTM, 1983.
[13] E.R. Parker, Brittle Behavior of Engineering Structures, John Wiley & Sons, 1957.
[14] H.W. Hayden, W.G. Moffatt, and J. Wulff, The Structure and Properties of Materials, Vol. III, John Wiley & Sons, 1965.
[15] A Guide for Fatigue Testing and the Statistical Analysis of Fatigue Data, ASTM STP-91-A, 1963.
[16] Anderson, T.L., Fracture Mechanics: Fundamentals and Applications, CRC Press, Boca Raton, 1991.
[17] Hertzberg, R.W., Deformation and Fracture Mechanics of Engineering Materials, Wiley, New York, 1976.
[18] Knott, J.F., Fundamentals of Fracture Mechanics, John Wiley – Halsted Press, New York, 1973.
[19] Strawley, J.E., and W.F. Brown, Fracture Toughness Testing, ASTM STP 381, 133, 1965.